Journal of Functional Materials and Applied Engineering

Research Paper

# Preparation of metal organic framework materials and their adsorption performance for heavy metal $Cr^{6+}$ ions in wastewater treatment process

**Srabani Campbell[1,*], Roberto Ahmad[1], Vlastimil Sholl[2]**

[1] Institute of Chemistry, Military University of Technology, 00-908, Warsaw, Poland
[2] Chemical Engineering Department, Faculty of Engineering, Ferdowsi University of Mashhad, Mashhad, Iran
*Corresponding author: campbell@wat.edu.pl

**Abstract.** The heavy metal containing wastewater discharged from industries such as leather and smelting is toxic and difficult to degrade, which not only endangers human health but also causes serious damage to the ecological environment. The use of simple, efficient, and low-cost technologies to treat pollutants in such wastewater has gradually become a research focus both domestically and internationally. MOFs are cutting-edge porous solids that marry ultra-high surface areas and tunable porosity with architecturally adjustable frameworks and a wealth of open metal centers. They have broad development prospects in adsorption, separation, energy storage, catalysis, and other fields. Indium based MOF materials are composed of octahedral units formed by In3+ions connected to organic ligands, and have good structural and thermal stability. However, there is currently limited research on the preparation of In MOF series materials and their application in industrial wastewater pollutant treatment. Using sodium citrate as a modifier, the synthesized MIL-68 (In) was modified to obtain indium based material MIL-68 (In) - SC. The structural parameters of the modified material were measured to determine the appropriate concentration and dosage of the modifier. Introducing the modifier markedly expanded the scaffold's surface; after dosing 0.2 mL of 0.5 M sodium citrate, MIL-68(In)-SC delivered a BET area of 1164.91 $m^2 g^{-1}$—56.6 % larger than its unmodified parent. The same trio of frameworks was then benchmarked for Cr(vi) sequestration from aqueous media.The results showed that all three materials had adsorption effects on heavy metal Cr6+ions, with adsorption rates and capacities of 30.05% and 24.04mg/g, respectively.

**Keywords:** *Metal organic framework materials; Sewage; adsorbent; Cr6+*

Received on 02 April 2024, Accepted on 02 June 2024, Published on 15 July 2024



## 1 Introduction

Heavy metal wastewater represents a major category of industrial effluent. Pollution arises not only from industrial production discharges but also from heavy metal products in domestic waste and light industries such as papermaking and jewelry processing [1]. Heavy industry, due to its diversity, complex scenarios, and large discharge volumes, is a key contributor to heavy metal pollution. The rapid development of sectors like mining, metallurgy, tanning, and electroplating has led to a high incidence of heavy metal pollution [2]. Heavy metals are typically defined as metallic elements exhibiting a density exceeding 4.5 $g/cm^3$ under standard temperature and pressure, with representative examples encompassing copper (Cu), nickel (Ni), mercury (Hg), lead (Pb), chromium (Cr), and cadmium (Cd) [3]. Heavy metal wastewater is highly toxic, non-biodegradable, and difficult to treat. Direct discharge into the environment contaminates surface water resources, can cause death of aquatic organisms [4], and through infiltration, can affect soil and even groundwater quality [5]. Heavy metals are prone to bioaccumulation. Long-term human exposure or consumption of contaminated plants and animals leads to accumulation in the body, as they cannot be metabolized and excreted, eventually causing significant damage to the nervous system and organs [6].

Chromium (Cr) is a typical heavy metal pollutant, primarily originating from electroplating workshops, dyeing factories, and tanneries, which generate large amounts of wastewater during processing and manufacturing [7-9]. Common valence states are trivalent ($Cr^{3+}$) and hexavalent ($Cr^{6+}$). Chromium ions can enter the human body through respiration, contact, and food, leading to respiratory tract, nasopharyngeal, and digestive tract diseases.

Chromium ions also possess carcinogenic potential, potentially inducing cancer [10]. Compared to $Cr^{3+}$, $Cr^{6+}$ is more toxic, more easily absorbed by the human body, and causes long-term harm. The national limit for Cr(vi) in potable water is set at 0.05 mg $L^{-1}$ [11], yet industrial effluents frequently carry chromium levels hundreds to thousands of times higher, grossly surpassing the legal discharge threshold. Therefore, researching effective methods to reduce $Cr^{6+}$ ion concentration in wastewater is crucial.

To mitigate the increasing environmental pollution and health hazards caused by $Cr^{6+}$ ions, researchers continuously explore heavy metal treatment technologies. Common methods include chemical precipitation, ion exchange, electrochemical treatment, and adsorption [12-15].

Chemical precipitation primarily works by adjusting the solution pH and adding precipitating agents to convert free or complexed heavy metal ions in wastewater into insoluble or poorly soluble heavy metal compounds, thereby separating them from the wastewater [15]. Depending on the precipitant used, it can be categorized into neutralization precipitation, sulfide precipitation, ferrite co-precipitation, and coagulation precipitation [16]. This involves adding chemicals like sulfides or flocculants to the wastewater, causing the heavy metal ions to settle, followed by filtration of the precipitate to purify the water. For $Cr^{6+}$ removal, reducing agents like $FeSO_4$, $Na_2SO_3$, or $NaHSO_3$ are added to reduce $Cr^{6+}$ to $Cr^{3+}$, followed by alkaline substances like NaOH or $Ca(OH)_2$ to form $Cr(OH)_3$ precipitate [17]. However, chemical precipitation often requires large amounts of reagents, potentially introducing new pollutant ions, and the treated effluent may not meet standards, making it unsuitable as a final treatment step.

Ion exchange utilizes ion exchange resins to selectively exchange metal anions in the water, followed by resin regeneration or disposal, to remove heavy metals [18]. Early studies used natural resins; later, synthetic resins were developed for improved functionality and performance. Anion exchange resins can exchange $CrO_4^{2-}$ and $Cr_2O_7^{2-}$ ions, while cation exchange resins can remove $Cr^{3+}$ or other metal cations [19-20]. Resins are non-toxic, have high treatment capacity, can handle multiple metal ions, and cause minimal secondary pollution. However, they require high-quality influent and resins, have a large footprint, long treatment cycles, and are unsuitable for large-scale applications.

Electrochemical methods use electrical current to drive reactions like decomposition, oxidation-reduction, and flotation for toxic heavy metal removal [25]. These methods offer simple equipment, potential for automation, and low secondary pollution, showing good application prospects due to their versatility [21]. Reactor efficiency depends on electrode materials and parameters like mass transfer efficiency, current density, and wastewater composition. However, high consumption of electrode materials and electricity, significant operating costs, complex maintenance, and low mass transfer efficiency limit their application [22].

Adsorption utilizes the porous structure of materials to remove heavy metals through mechanisms like electrostatic attraction, surface complexation, and ion exchange, followed by adsorbent removal [23]. Adsorption includes physical adsorption, chemical adsorption, and biosorption. Physical adsorption relies on the adsorbent's structure; chemical adsorption involves chelation with functional groups; biosorption uses microorganisms or algae to accumulate metal ions. Overall, adsorption is simple, requires less sophisticated equipment, and is highly efficient, proving very effective for treating both methylene blue and $Cr^{6+}$ ions in wastewater [24]. The type and performance of the adsorbent are critical. Traditional adsorbents like molecular sieves, zeolites, activated resins, and activated carbon have certain effectiveness but are limited in wastewater treatment due to high production costs, difficult regeneration, and potential for secondary pollution. Lately, MOFs have stepped into the spotlight as a new generation of adsorbents, sparking fresh optimism for high-performance wastewater cleanup [25].

In recent years, MOFs have been increasingly applied in liquid-phase adsorption and separation, particularly for treating dye molecules, aromatic organic compounds, and heavy metal ions in wastewater. Typical dye pollutants—methyl orange, methylene blue, Congo red and rhodamine B—are frequent culprits in textile effluent. A recent study [26] prepared UiO-66-Cl and benchmarked it against activated carbon and bagasse: across 10–1000 mg $L^{-1}$ the MOF delivered maximum uptakes of 94 mg $g^{-1}$ for rhodamine B and 152 mg $g^{-1}$ for Congo red, dwarfing the conventional sorbents and underscoring its practical promise. Other researchers [27] used sodium acetate as a modulator to prepare MIL-68(In) nanorods with high surface area based on the classic

MIL-68(In). Against Congo red, the engineered variant peaked at 1204 mg $g^{-1}$—an order-of-magnitude leap over the classic benchmark—highlighting its exceptional scalability. Treating toxic aromatic compounds like phenol and benzenesulfonic acid is crucial. $NH_2$-MIL-53(Al) synthesized solvothermally showed good adsorption for diclofenac sodium under acidic and neutral conditions [28]. Using MIL-68(In) and $NH_2$-MIL-68(In) to adsorb sulfanilic acid, studies reported that the mechanism involves synergistic π-π stacking and hydrogen bonding. The introduction of amino groups significantly enhanced hydrogen bonding, enabling $NH_2$-MIL-68(In) to achieve an adsorption capacity of 401.6 mg/g [29]. Additionally, using UiO-66(Zr) as an adsorbent for toxic metal ions like $Zn^{2+}$, $Bi^{3+}$, $Hg^{2+}$, $Pb^{2+}$, and $Cd^{2+}$ showed that different ions have optimal adsorption conditions [30].

This work targets solvothermal fabrication of MIL-68(In) and $NH_2$-MIL-68(In) from hydrated indium nitrate and terephthalic-acid-type linkers, followed by citrate-mediated modification to yield ultra-high-surface-area MIL-68(In)-SC. The adsorption performance of these materials, both before and after modification, for methylene blue (MB) and heavy metal $Cr^{6+}$ ions in wastewater will be investigated.

## 2 Materials and methods

### 2.1 Preparation of MIL-68 (In)

MIL-68(In) was synthesized solvothermally by mixing hydrated indium nitrate, terephthalic acid ($H_2BDC$) and DMF in a Teflon-lined autoclave, followed by homogeneous stirring to ensure complete dispersion before heating. Then, the reaction kettle was placed in an oven, heated to 100 ℃ for 48 hours, cooled, and centrifuged to obtain white MIL-68 (In) initial product; Wash the obtained initial product several times with DMF and anhydrous ethanol, then activate it in anhydrous ethanol for three days. After centrifugal separation, the solid was vacuum-dried at 60 °C for 12 h to yield MIL-68(In) as a white, free-flowing powder.

### 2.2 Preparation ofNH2-MIL-68 (In)

Starting from the as-synthesized MIL-68(In), amino functionality was grafted onto the framework to afford the derivative $NH_2$-MIL-68(In) [66,72]. To install $–NH_2$ handles, the linker was switched directly to 2-aminoterephthalic acid ($NH_2$-$H_2BDC$). In a typical run, $In(NO_3)_3{\cdot}xH_2O$ and $NH_2$-$H_2BDC$ were dissolved in DMF inside a Teflon vessel, heated at 125 °C for 5 h under autogenous pressure, cooled, centrifuged, and collected as a pale-yellow $NH_2$-MIL-68(In) crude solid. The sentence is:; Wash the initial product several times with DMF and anhydrous ethanol, then activate it in anhydrous ethanol for three days. After centrifugation, the product was vacuum-dried at 60 °C for 12 h to yield $NH_2$-MIL-68(In) as a pale-yellow powder.

### 2.3 Preparation of MIL-68 (In) - SC

Based on the preparation process of MIL-68 (In), sodium citrate solution was added during the raw material mixing process, and modified MIL-68 (In) - SC was prepared by solvothermal synthesis: Indium nitrate hydrate, terephthalic acid, and DMF were mixed in a polytetrafluoroethylene reaction vessel in a ratio of 2.2.1, stirred evenly, and a certain amount of sodium citrate solution was slowly added to the mixture to continue stirring. After mixing evenly, the reaction vessel was placed in an oven and heated to 100 ℃ under its own pressure for 0.5 hours. After cooling, the white MIL-68 (In) - SC initial product was obtained by centrifugation; Wash the initial product of MIL-68 (In) - SC several times with DMF and anhydrous ethanol, replace it with anhydrous ethanol for three days, centrifuge and vacuum dry at 60 ℃ for 12 hours, and finally obtain MIL-68 (In) - SC as a white powder.

### 2.4 Material Characterization and Analysis Methods

#### 2.4.1 X-ray Powder Diffraction (XRD)

Crystallinity was assessed on a Rigaku D/max-2500 powder X-ray diffractometer (60 kV, 300 mA) using a 2θ sweep from 5° to 40° at 10° $min^{-1}$.

#### 2.4.2 Nitrogen Isothermal Adsorption Desorption Instrument

*DOI:*

Textural properties—BET surface area, pore volume and pore size—were extracted from $N_2$ physisorption isotherms collected on a Quantachrome Autosorb IQ analyzer. The sample needs to be vacuum dried at 100 ℃ for 12 hours before measurement, and then analyzed under 77K liquid nitrogen. The required data can be calculated by DFT model.

#### 2.4.3 Fourier transform infrared spectroscopy (FT-IR)

MOFs host a variety of functional moieties, each absorbing at characteristic wavenumbers, bandwidths and intensities; FT-IR was therefore employed to fingerprint these groups and confirm the molecular makeup of the frameworks.

Using the WQF-510 Fourier transform infrared spectrometer from Beijing Raleigh Company, the materials adjusted with amino groups and sodium citrate were analyzed. By detecting and comparing the characteristic peaks of functional groups, it was confirmed whether the introduction of functional groups was successful.

### 2.5 Adsorption Performance Experiment and Analysis Method

The static experimental method was used to adsorb Cr6+ions in water. Different concentrations of Cr6+ion solutions used in the experiment were diluted with 100mg/L standard solution. Identical analytical protocols were applied to MIL-68(In), $NH_2$-MIL-68(In) and MIL-68(In)-SC throughout the study. The experimental procedure is as follows: prepare a certain concentration of Cr6+ion solution, take 20mL of Cr6+ion solution and place it in multiple 100mL stoppered conical flasks, then add 5mg of adsorbent to each flask. Afterwards, place the stoppered conical flasks in a constant temperature oscillator and perform oscillatory adsorption at a certain speed (150rpm). During the experiment, keep the oscillator temperature and speed constant. Explore the effects of different adsorption times (0~720mim), solution pH values (2~11), initial concentrations (5~40mol/L), and adsorbent dosage (1~11mg) on the adsorption performance of Cr6+ion solution.

After adsorption is completed, the solution is filtered using an organic filter membrane. Filtrate absorbance was read on a UV spectrophotometer, its concentration back-calculated from a pre-established calibration curve, and both removal efficiency and uptake capacity were subsequently computed via standard equations.

## 3. Results and Discussion

### 3.1 X-ray Powder Diffraction (XRD) Analysis

Figure 1 displays the powder X-ray diffraction patterns of the as-synthesized MIL-68(In), $NH_2$-MIL-68(In), and MIL-68(In)-SC-11 frameworks.

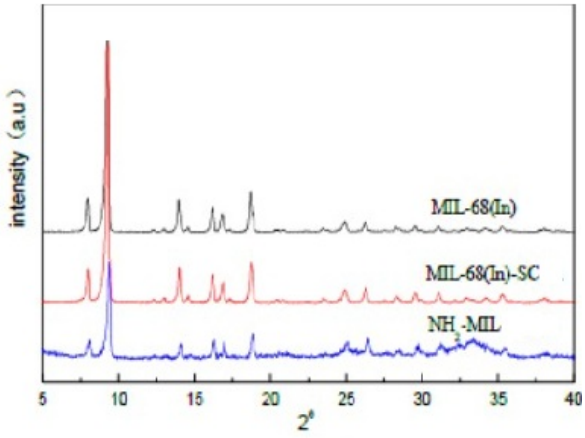


**Figure 1** XRD patterns of three synthetic materials

*DOI:*

According to Figure 3-1, the three synthetic materials exhibit characteristic diffraction peaks at 8 °, 9.26 °, 13.96 °, 16.22 °, and 18.68 °, which are consistent with the diffraction peak data of MIL-68 (In) in reference [66], indicating that the synthetic material is an indium based MOF material. The diffraction peak positions of the three materials are basically consistent, indicating that the introduction of carboxyl groups in amino and sodium citrate did not affect the topological structure of the materials; The diminished peak intensities observed for $NH_2$-MIL-68(In) reveal that amino-group incorporation lowers the overall crystalline order of the framework. The XRD patterns of MIL-68 (In) - SC-11 and MIL-68 (In) are almost identical, with sharp peaks, indicating that the synthesized material has high crystallinity and the addition of sodium citrate does not change the crystal structure of the synthesized material [31].

### 3.2 Specific surface area and pore size (DFT) analysis

Figure 2(a) presents the $N_2$ sorption isotherms of MIL-68(In), $NH_2$-MIL-68(In) and MIL-68(In)-SC-11. MIL-68(In) exhibits a Type-I profile, confirming its microporous character. NH2-MIL-68 (In) shows a mixed curve of type I and IV, with an H3 hysteresis loop, indicating that NH2-MIL-68 (In) is a micro mesoporous mixed pore material with a narrow pore structure and uneven distribution of pore shape and size [32]; MIL-68 (In) - SC-11 is an I-type curve, exhibiting a microporous structure. N2 molecules can effectively diffuse into the pores of the three synthetic materials for adsorption. MIL-68(In)-SC-11 outperforms both MIL-68(In) and $NH_2$-MIL-68(In) in uptake, a direct consequence of its enlarged surface area that provides more accessible sites for guest binding. Figure 2(b) (labeled 3-3) reveals that MIL-68(In) displays a sharp, narrow distribution centered at ~1.9 nm, indicative of uniform micropores. $NH_2$-MIL-68(In) exhibits a narrow distribution centered at ~2 nm, showing that amino functionalization slightly enlarges the average pore size. In contrast, MIL-68(In)-SC-11 displays two distinct peaks between 1 and 2 nm, typical of microporous solids [33], and its cumulative pore volume markedly exceeds that of both parent and amino-tagged analogues, offering expanded space for guest uptake.

Table 1 summarizes the BET surface area, pore diameter, and pore volume of MIL-68(In), $NH_2$-MIL-68(In), and MIL-68(In)-SC-11, confirming that each framework possesses a high-surface-area, porous architecture. MIL-68(In) exhibits a BET surface area of 743.72 $m^2 g^{-1}$, a pore volume of 0.42 $cm^3 g^{-1}$, and an average pore diameter of 1.96 nm. $NH_2$-MIL-68(In) displays a BET surface area of 726.12 $m^2 g^{-1}$, a pore volume of 0.38 $cm^3 g^{-1}$, and an average pore width of 2.04 nm. MIL-68(In)-SC-11 reaches a BET area of 1164.91 $m^2 g^{-1}$ with 0.56 $cm^3 g^{-1}$ pore volume and 1.63 nm pores. While $NH_2$-MIL-68(In) shows only a marginal gain over MIL-68(In), the amino tag nevertheless enlarges the mean pore size. Despite its slightly smaller pores, MIL-68(In)-SC-11 couples an exceptionally high surface area with expanded pore volume, underscoring the pronounced influence of sodium-citrate modification on framework architecture [34] and, consequently, on its enhanced uptake capability and practical utility.

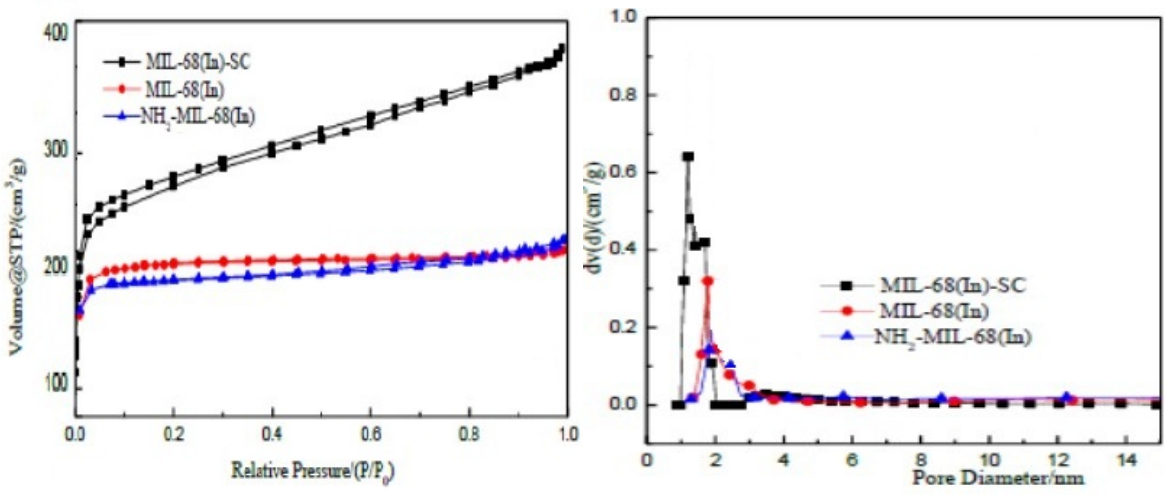


**Figure 2** N2 adsorption desorption isotherms and pore size distribution of three materials

Table 1 Structural Parameters of Three Synthetic Materials

| materials | $S_{BET}/(m^2 \cdot g^{-1})$ | $V/(cm^3 \cdot g^{-1})$ | D/(nm) |
|---|---|---|---|
| MIL-68(In) | 743.72 | 0.42 | 1.96 |
| $NH_2$-MIL-68(In) | 726.12 | 0.38 | 2.04 |
| MIL-68(In)-11 | 1164.91 | 0.56 | 1.63 |

### 3.3 Fourier transform infrared spectroscopy (FT-IR) analysis

FT-IR spectra of MIL-68(In), $NH_2$-MIL-68(In) and MIL-68(In)-SC-11 are displayed in Figure 3-5.According to Figure 3, the large peak at 3446cm-1 in the spectra of the three synthetic materials is the O-H vibration signal in free water on the crystal surface; The vibration signals of the functional groups on the organic ligand during two stretching vibrations between 1300 and 1700 cm-1, including C=O and C-O in the carboxyl group [35]; The vibration signals near 1700 and 1280cm-1 may be C=O and C-N vibrations on residual DMF solvent [36]. $NH_2$-MIL-68(In) and MIL-68(In)-SC-11 retain the core vibrational pattern of the parent framework, confirming that functionalization leaves the backbone intact. A new band at ~1250 $cm^{-1}$ in $NH_2$-MIL-68(In) evidences successful $–NH_2$ incorporation, while MIL-68(In)-SC-11 shows markedly intensified twin peaks between 1300–1700 $cm^{-1}$, signaling a higher density of carboxyl signatures. Citrate is a carboxylate salt whose delocalized π-system generates an asymmetric $COO^-$ stretch at 1550–1650 $cm^{-1}$; the clear band in this window [37] confirms successful carboxyl grafting.

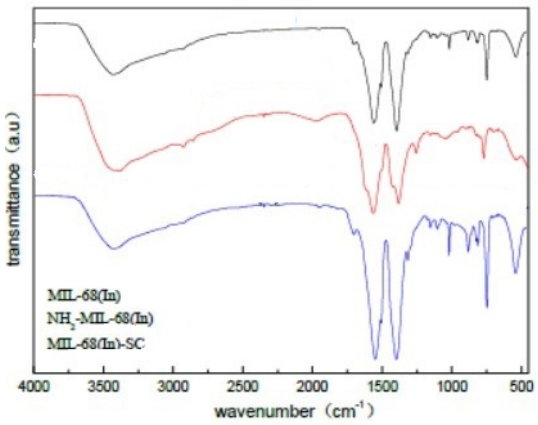


**Figure 3** FT-IR spectra of three synthetic materials

### 3.4 Study on $Cr^{6+}$ Adsorption by MOF Materials

#### 3.4.1 The Influence of pH Value on Adsorption Performance

Solution pH is a critical lever in heavy-metal uptake: it dictates both the speciation of the metal ion and the surface charge of the sorbent and sorbate [76]. For each trial, 20 mL of 20 mg $L^{-1}$ Cr(vi) solution was transferred to a 100 mL Erlenmeyer flask and sealed. The Cr(vi) medium was stepwise adjusted to pH 2, 3, 4, 5.4 (as-is), 7, 8, 9, 10 and 11 with 1 M HCl or NaOH. Add 5mg of adsorbent to each flask, and then place the stoppered conical flask into a constant temperature (25 ℃) oscillator. The oscillation speed remains constant and the oscillation time is 90 minutes. Following equilibration, the supernatant was withdrawn with a syringe, passed through a 0.45 μm hydrophilic membrane, and analyzed for residual Cr(vi). Figure 4 summarizes the pH-dependent uptake of Cr(vi) by MIL-68(In), $NH_2$-MIL-68(In) and MIL-68(In)-SC-11 under these standardized conditions.

Figure 4 demonstrates that solution pH exerts a pronounced influence on the Cr(vi) uptake efficiency of all three MOF adsorbents. Over pH 2–4 MIL-68(In) removal climbs from 19 % to 25.5 %, but beyond pH 4 the trend reverses, falling back to 21 % at pH 11; hence the optimum window for this framework is pH 4, where 25.5 % of Cr(vi) is sequestered. $NH_2$-MIL-68(In) shows a steady rise from 17.8 % (pH 2) to a maximum of 29.2 % at pH 9, then slips to 23.2 % at pH 11, establishing pH 9 as its optimum. MIL-68(In)-SC-11 mirrors the parent trend: removal jumps from 21.1 % to 28.0 % as pH moves from 2 to 3. When the pH increases from 3 to 11, the

adsorption rate continues to decrease to 16.48%, that is, the pH value is 3. MIL-68 (In) - SC-11 has the best adsorption effect on Cr6+ions, with a maximum adsorption rate of 27.98%. By comparing the adsorption rates of three materials, the addition of amino groups and sodium citrate modification improved the adsorption rate of the synthesized material [38].

For amino modified NH2-MIL-68 (In), when the acidity is strong, the H+content in the solution is high, and the surface of the adsorbent is prone to undergo amino protonation reactions, increasing the number of positive charges on the adsorbent surface and generating electrostatic repulsion with Cr6+ions, which is not conducive to adsorption; As pH rises the $H^+$ reservoir is depleted, suppressing amino protonation and steadily lowering the net positive surface charge of the sorbent. Higher alkalinity enriches negative surface sites, promoting electrostatic attraction toward anionic Cr(vi) species and boosting uptake. However, strong acidity and alkalinity can damage the material structure and affect the adsorption effect. For MIL-68 (In) - SC-11 (MIL-68 (In) - COONa) modified with sodium citrate, under strong acid conditions, the H+ion content increases, promoting the conversion of the - COONa group to - COO -. Carboxyl groups can chelate with metal ions, allowing for ion exchange during the adsorption process. The carboxyl CO - system of carboxylate salts has a multi electron π - bond system, with negative charges dispersed on two oxygen atoms and one carbon, enhancing electrostatic interactions and facilitating the migration of metal ions, thereby promoting adsorption; In strongly alkaline media the abundance of $OH^-$ hinders $–COO^-$ formation and can block active sites, diminishing overall Cr(vi) removal [39].

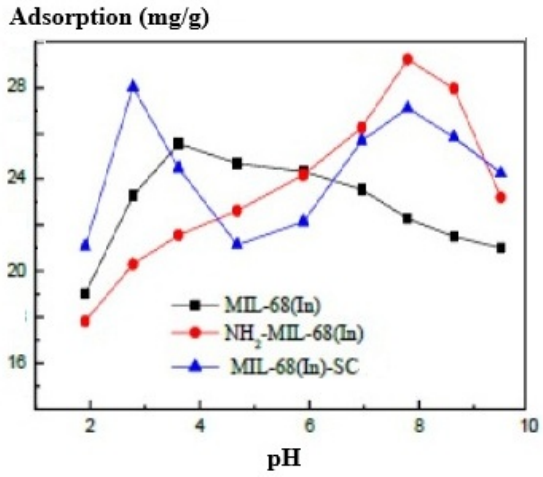


**Figure 4** The Effect of pH Value on the Adsorption Performance of Synthetic Materials

**3.4.2 The Effect of Adsorption Time on Adsorption Performance**

From the foregoing data, the optimal pH for each sorbent was fixed; all other parameters were kept as in Section 5.1. Uptake kinetics were then tracked at 15, 30, 60, 90, 120, 150 and 180 min, with the outcomes plotted in Figure 5.

From Figure 5, it can be seen that the adsorption rates of the three synthetic materials first show an upward trend with the increase of time, and then gradually approach equilibrium. Both MIL-68(In) and MIL-68(In)-SC-11 exhibit a steep rise in removal efficiency within the first 60 min, followed by a more gradual increment between 60 and 120 min. After 120 minutes of reaction, the material's adsorption rate for Cr6+ions tends to stabilize. The adsorption rate of NH2-MIL-68 (In) increases rapidly with time 60 minutes before the reaction, and increases slowly within 60-90 minutes. Equilibrium is effectively reached at 90 min, roughly half an hour sooner than the plateau observed for the parent and citrate-modified frameworks. Optimal contact times are 120 min for MIL-68(In), 90 min for $NH_2$-MIL-68(In) and 120 min for MIL-68(In)-SC-11, yielding equilibrium removals of 27.1 %, 29.2 % and 30.0 %, respectively.

At the outset, the elevated metal concentration combines with fully accessible external and internal surfaces,

providing an abundance of vacant active sites that drive rapid initial uptake. The adsorption driving force is strong, making the adsorption process relatively easy to carry out. Therefore, the adsorption rate increases rapidly in a short period of time. Afterwards, the number of empty pores decreases, and the metal ions in the adsorbent hinder the entry of metal ions in the solvent, resulting in slow adsorption and ultimately reaching equilibrium. Post-synthetic grafting of $–NH_2$ or –COOH moieties onto $NH_2$-MIL-68(In) and MIL-68(In)-SC-11, respectively, amplifies electrostatic interactions and accelerates Cr(vi) binding. Additionally, MIL-68(In)-SC-11 offers a markedly larger surface area than both MIL-68(In) and $NH_2$-MIL-68(In), translating into superior overall uptake.

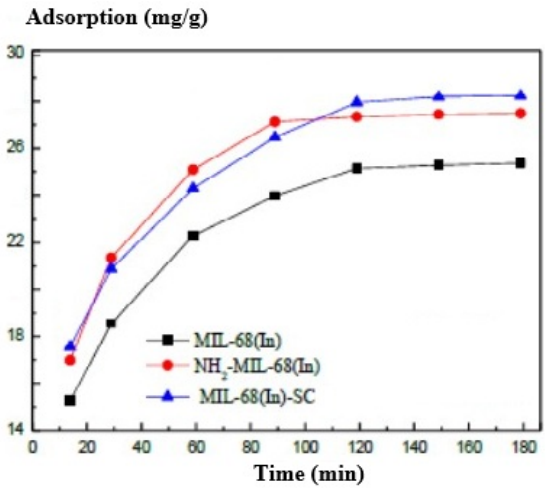


**Figure 5** The Effect of Adsorption Time on the Adsorption Performance of Synthetic Materials

### 3.4.3 Effect of Cr6+ion concentration on adsorption performance

Guided by the kinetic data in Section 5.2, the optimal contact times were set at 120 min, 90 min and 120 min for MIL-68(In), $NH_2$-MIL-68(In) and MIL-68(In)-SC-11, respectively. All other adsorption conditions were the same as the experimental conditions in 5.2. The effects of Cr6+ion concentration on the adsorption rate and amount of the three materials were investigated at Cr6+ion concentrations of 5, 10, 15, 20, 25, 30, and 40mg/L. The results are shown in Figure 6.

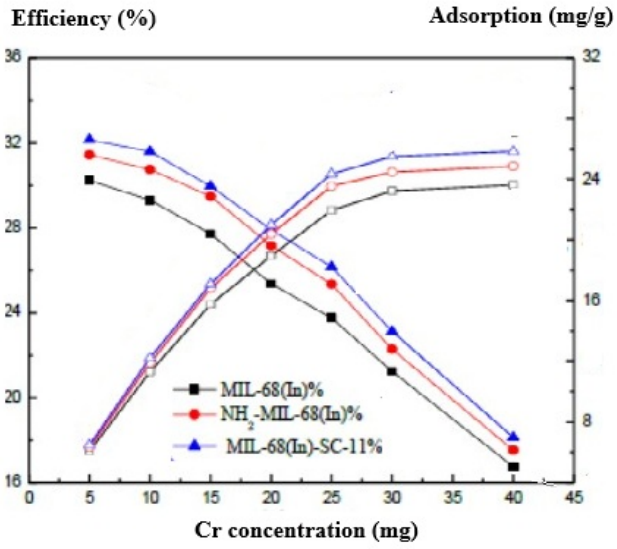


**Figure 6** Effect of Cr6+ion concentration on the adsorption performance of synthetic materials

Figure 6 illustrates that the initial Cr(vi) concentration strongly governs both removal efficiency and uptake density. For every MOF the percentage removed falls as the concentration rises, whereas the capacity climbs until it levels off. Specifically, MIL-68(In) removal drops from 32.8 % to 17.0 % while its loading rises from 6.6 mg $g^{-1}$ to a plateau near 26.7 mg $g^{-1}$. The adsorption rate of NH2-MIL-68 (In) decreased from 34.18% to 17.87%; The adsorption capacity increased from 6.85 mg/g to 28.59 mg/g and then tended towards equilibrium. The adsorption rate of MIL-68 (In) - SC-11 decreased from 35.03% to 18.57%; Capacity advanced from 7.01 mg $g^{-1}$ to 29.19 mg $g^{-1}$ before flattening out.

At fixed sorbent mass, higher Cr(vi) levels drive the solids toward saturation, capping further uptake; excessive concentrations block both external and internal sites, and accumulating unbound ions lower the apparent removal efficiency. Beyond mere physisorption, $NH_2$-MIL-68(In) and MIL-68(In)-SC-11 engage –$NH_2$ and –COOH sites in ion-exchange [40], boosting both rate and capacity.

**3.4.4 Effect of adsorbent dosage on adsorption performance**

Guided by the foregoing data, optimal pH and contact time were fixed for each MOF. To probe dosage effects, 20 mL aliquots of 20 mg $L^{-1}$ Cr(vi) were treated with 3, 5, 7, 9, 11, 20 or 30 mg of MIL-68(In), $NH_2$-MIL-68(In) or MIL-68(In)-SC-11; the resulting removal efficiencies and uptake capacities are plotted in Figure 7.

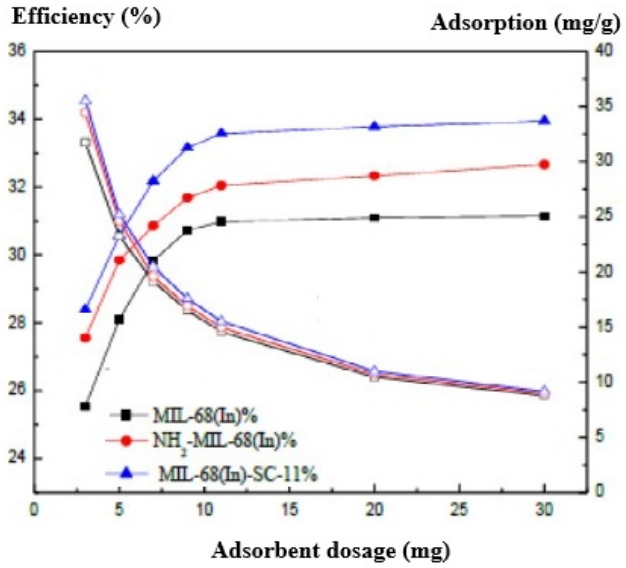


**Figure 7** Effect of adsorbent dosage on the adsorption performance of synthetic materials

Figure 7 shows that, at fixed Cr(vi) concentration, the percentage removed rises steadily with increasing sorbent mass until it plateaus, whereas the uptake capacity (mg $g^{-1}$) declines monotonically across the same dosage range. Below 9 mg the removal efficiency climbs steeply; between 9 and 11 mg the rise is modest; above 11 mg the curve flattens, signalling approach to saturation. Capacity drops sharply at low loadings, then tails off gradually as sorbent mass continues to rise.

At fixed Cr(vi) concentration, higher sorbent loadings supply extra pores, larger cumulative surface area and more active sites, so removal efficiency surges initially. Once the residual Cr(vi) concentration becomes vanishingly small, additional solid contributes little further uptake and the curve levels off. After reaching adsorption equilibrium, the adsorption rate no longer changes with the increase of adsorbent amount, and the agglomeration effect between adsorbent particles will also make the adsorption rate no longer significantly increase. With the Cr(vi) pool fixed, every extra gram of sorbent dilutes the uptake per unit mass, so capacity declines monotonically.

**3.4.5 Adsorption kinetics of Cr6+ions by MIL-68 (In) and modified materials**

Following Section 5.1, the Cr(vi) solution was pre-adjusted to its optimal pH. Aliquots (20 mL) were then charged with 5 mg of MIL-68(In), $NH_2$-MIL-68(In) or MIL-68(In)-SC-11 for comparative uptake tests. After adsorption for 15, 30, 60, 90, 120, 150, and 180 minutes, filter through a water-based filter membrane to obtain the filtered clear solution. After equilibration, the supernatant absorbance was read and the Cr(vi) uptake computed; capacity versus time data were plotted to yield the kinetic curves shown in Figure 8.

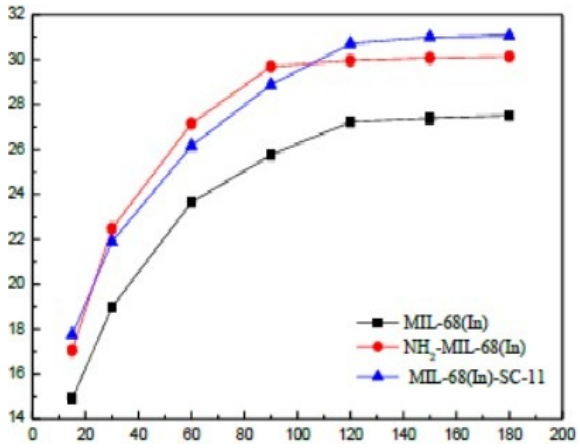


**Figure 8** Kinetic curves of Cr6+ion adsorption on MIL-68 (In), NH2-MIL-68 (In), and MIL-68 (In) - SC-11 materials

**3.4.6 Adsorption isotherms of Cr6+ions on MIL-68 (In) and modified materials**

Following the earlier optimization, the Cr(vi) solutions were first set to their respective optimal pH values. Separate 20 mL aliquots at 5, 10, 15, 20, 25, 30, 40 and 50 mg $L^{-1}$ were then dosed with 5 mg of MIL-68(In), $NH_2$-MIL-68(In) or MIL-68(In)-SC-11 for isotherm evaluation. Determine the adsorption equilibrium time of each material according to the experiment. Following equilibration, the suspensions were filtered through a 0.45 μm aqueous membrane, and the filtrate absorbance was measured to determine residual Cr(vi) concentrations. The uptake values were then plotted against equilibrium concentration to construct the adsorption isotherms shown in Figure 9.

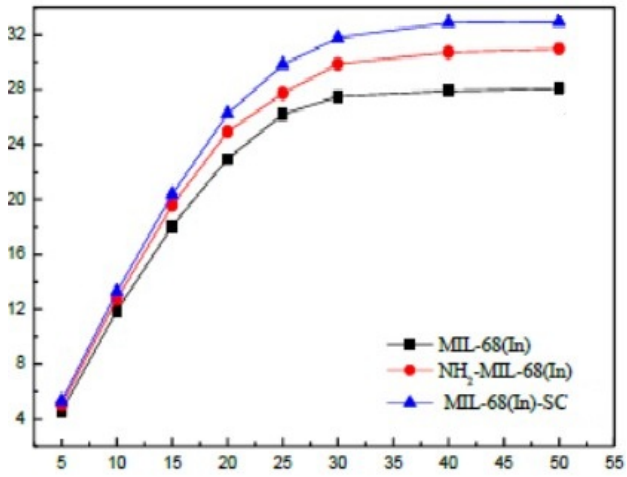


**Figure 9** Adsorption isotherms of Cr6+ions by three synthetic materials

From Figure 9, it can be seen that the adsorption of Cr6+ions by the three materials increases with concentration, and the adsorption capacity starts to increase rapidly, then increases slowly, and finally reaches adsorption equilibrium. MIL-68(In) approaches saturation near 25 mg $L^{-1}$ Cr(vi), whereas $NH_2$-MIL-68(In) and MIL-68(In)-SC-11 level off around 35 mg $L^{-1}$, marking their respective equilibrium concentrations.

## 4. Conclusion

This chapter presents a systematic investigation of Cr(vi) uptake by MIL-68(In), its amino-functionalised derivative $NH_2$-MIL-68(In), and the citrate-modified MIL-68(In)-SC-11. Key operational variables—solution pH, contact time, initial Cr(vi) concentration and sorbent dosage—were evaluated to map their influence on adsorption performance. The adsorption kinetics and isotherms of three materials were fitted through experimental data; And the regeneration performance of three materials for adsorption applications was investigated, and synthetic materials with excellent adsorption performance were screened.

Under the conditions of an adsorbent dose of 5mg and a Cr6+ion concentration of 20mg · L-1, with a solution pH of 4 and an adsorption time of 120min, the suitable adsorption conditions for MIL-68 (In) are achieved, with an adsorption rate of 27.06% and an adsorption capacity of 21.76 mg/g; Optimal uptake for $NH_2$-MIL-68(In) is attained at pH 9 and 90 min, delivering 29.2 % removal and a loading of 23.5 mg $g^{-1}$. MIL-68(In)-SC-11 performs best at pH 3 and 120 min, reaching 30.1 % removal and a capacity of 24.8 mg $g^{-1}$. In short, grafting amino or carboxyl functionalities boosts Cr(vi) uptake; the enlarged surface area and pore volume of MIL-68(In)-SC-11 render it the most effective sorbent of the series.

## References

[1] Deng Y., Zhao R., Advanced oxidation processes (AOPs) in wastewater treatment[J]. Current Pollution Rep orts, 2015, 1: 167-176.

[2] Zornoza B., Tellez C., Coronas J., et al. Metal organic framework based mixed matrix membranes: an incre asingly important field of research with a large application potential[J]. Microporous & Mesoporous Mate rials, 2013, 166: 67-78.

[3] Eba C., Aea C., Mab C., et al. Synthesis and characterization of nano-sized metal organic framework-5 (MO F-5) by using consecutive combination of ultrasound and microwave irradiation methods[J]. Inorganica Ch imica Acta, 2019, 485: 118-124.

[4] Priscilla R. B., Carla M. B., Verónica P., et al. The metal-organic framework HKUST-1 as efficient sorbent in a vortex-assisted dispersive micro solid-phase extraction of parabens from environmental waters, cosmet ic creams, and human urine[J]. Talanta, 2015, 139: 13-20.

[5] Sun C. Y., Qin C., Wang C. G., et al. Chiral nanoporous metal-organic frameworks with high porosity as ma terials for drug delivery[J]. Advanced Materials, 2011, 23(47): 5629-5632.

[6] Ferey, G., Mellot-Draznieks C., Serre C., et al. A Chromium Terephthalate-Based Solid with Unusually Larg e Pore Volumes and Surface Area[J]. Science, 2005, 309(5743): 2040-2042.

[7] X. Xu, B.Yan. Intelligent Molecular Searcher from Logic Computing Network Based on Eu(III) Functionalize d UMOFs for Environmental Monitoring. Advanced Functional Materials, 2017, 27(23): 247

[8] Krishnan S., Rawindran H., Sinnathambi C. M., et al. Comparison of various advanced oxidation processes used in remediation of industrial wastewater laden with recalcitrant pollutants[J]. Iop Conference, 2017, 206: 012089.

[9] Abazari., Reza M., Ali Slawin., et al. Morphology and size-controlled synthesis of a metal-organic framewo rk under ultrasound irradiation: an efficient carrier for pH responsive release of anti-cancer drugs and the ir applicability for adsorption of amoxicillin from aqueous solution[J]. Ultrasonics Sonochemistry, 2018, 4 2: 594-608.

[10] Y. L.Wu, G. P.YANG, X.ZHOU, et al. Three New Luminescent Cd(ii)-MOFs by Regulating The Tetracarboxyla te And Auxiliary Co-lLigands, Displaying High Sensitivity for Fe3+in Aqueous Solution. Dalton Transactions, 2015,44:10385-10391

[11] Li, H., Eddaoudi, M., O'Keeffe, M., et al. Design and synthesis of an exceptionally stable and highly porous metal-organic framework[J]. Nature, 1999, 402(6759): 276-279. [12] Zhang Z., Zhao Y., Gong Q., et al. MO Fs for CO2 capture and separation from flue gas mixtures: the effect of multifunctional sites on their adso rption capacity and selectivity[J]. Chemical Communications, 2013, 49(7): 653-661.

[12] C. VOLKRINGER, M.MEDDOURI, T.LOISEAU, et al. The Kagomé Topology of The Gallium And Indium Metal-Organic Framework Types With AMIL-68 Structure: Synthesis, XRD, Solid-State NMR Characterizations, Hy drogen Adsorption. Inorganic Chemistry, 2008, 47(24): 11892-11901

[13] Dhakshinamoorthy A., Asiri A. M., Garcí H., Metal-organic framework (MOF) compounds: photocatalysts f or redox reactions and solar fuel production[J]. Angewandte Chemie, 2016, 55(18): 5414-5445.
[14] Chan Q., Stroud R., Martins Z., et al. Concerns of Organic Contamination for Sample Return Space Mission s[J]. Space Science Reviews, 2020, 216(4):1-40.
[15] Chui S. S., Lo S. M., Charmant, J. P., et al. A Chemically Functionalizable Nanoporous Material [Cu3(TMA)2 (H2O)3]n[J]. Science, 1999, 283: 1148-1150.
[16] Zhang M., Feng G., Song Z., et al. Two-dimensional metal-organic framework with wide channels and resp onsive turn-on fluorescence for the chemical sensing of volatile organic compounds[J]. Journal of the Ame rican Chemical Society, 2014, 136(20): 7241-7244.
[17] Duarte C. L., Sampa M., Rela P. R., et al. Advanced oxidation process by electron-beam-irradiation-induce d decomposition of pollutants in industrial effluents[J]. Radiation Physics & Chemistry, 2002, 63(3): 647-6 51.
[18] Rasheed T., Hassan A. A., Bilal M., et al. Metal-organic frameworks based adsorbents: A review from remo val perspective of various environmental contaminants from wastewater[J].Chemosphere, 2020, 259: 127 369.
[19] Crini G., Non-conventional low-cost adsorbents for dye removal: a review[J]. Bioresource Technology, 200 6, 97(9): 1061-1085.
[20] Asgher M., Bhatti H. N., Mechanistic and kinetic evaluation of biosorption of reactive azo dyes by free, im mobilized and chemically treated Citrus sinensis waste biomass[J]. Ecological Engineering, 2010, 36(12): 1 660-1665.
[21] Wang Y J., Song J., Zhao W., et al. In situ degradation of phenol and promotion of plant growth in contami nated environments by a single Pseudomonas aeruginosa strain[J]. Journal of Hazardous Materials, 2011, 192(1): 354-360.
[22] Briceno G., Fuentes M. S., Saez J. M., et al. Streptomyces genus as biotechnological tool for pesticide degr adation in polluted systems[J]. Critical Reviews in Environmental Science and Technology, 2018, 48(10-1 2): 773-805.
[23] Qin Y., Hao M., Wang D., et al. Post-synthetic modifications (PSM) on metal-organic frameworks (MOFs) f or visible-light-initiated photocatalysis[J]. Dalton Transactions, 2021, 50(38): 13201-13215
[24] Li S., Zhang X., Huang Y., Zeolitic imidazolate framework-8 derived nanoporous Carbon as an effective and recyclable adsorbent for removal of ciprofloxacin antibiotics from water[J]. Journal of Hazardous Materia ls, 2017, 321(5): 711-719.
[25] Ye S., Zeng G., Wu H., et al. Co-occurrence and interactions of pollutants, and their impacts on soil remedi ation - a review[J]. Critical Reviews in Environmental Science & Technology, 2017, 47(16): 1528-1553.
[26] Jose V., Ros L., Ramón M. M., et al. Highly Selective Chromogenic Signaling of Hg2+ in Aqueous Media at Nanomolar Levels Employing a Squaraine-Based Reporter[J]. Inorganic Chemistry, 2004, 43(17): 5183-518 5.
[27] Zajda M., Aleksander-Kwaterczak U., Wastewater treatment methods for effluents from the confectioner y industry - an overview[J]. Journal of Ecological Engineering, 2019, 20(9): 293-304.
[28] Mohapatra S., Siddamallaiah L., Matadha N. Y., Behavior of acetamiprid, azoxystrobin, pyraclostrobin, and lambda-cyhalothrin in/on pomegranate tissues[J]. Environmental Science and Pollution Research, 2021, 2 8(22):27481-27492.
[29] Song T., Zhang P. Y., Zeng J., et al. Tunable conduction band energy and metal-to-ligand charge transfer fo r wide-spectrum photocatalytic H2 evolution and stability from isostructural metal-organic frameworks[J]. International Journal of Hydrogen Energy, 2017, 42(43): 26605-26616.
[30] Li H. J., Zhang N., He X. L., et al. Modulation of TEA and methanol gas sensing by ion-exchange based on a sacrificial template 3D diamond-shaped MOF[J]. Sensors and Actuators B Chemical, 2020, 315: 128-136.
[31] Abazari R., Mahjoub A. R., Amine-Functionalized Al-MOF#@yx Sm2O3-ZnO: A Visible Light-Driven Nanoco mposite with Excellent Photocatalytic Activity for the Photodegradation of Amoxicillin[J]. Inorganic Chemi stry, 2018, 57(5): 2529-2545.
[32] Brozek C. K., Dinca M., Lattice-imposed geometry in metal-organic frameworks: lacunary Zn4O clusters in MOF-5 serve as tripodal chelating ligands for Ni2+[J]. Chemical Science, 2012, 3(6): 2110-2113.
[33] He H. B., Li B., Dong J. P., et al. Mesostructured Nanomagnetic Polyhedral Oligomeric Silsesquioxanes (PO SS) Incorporated with Dithiol Organic Anchors for Multiple Pollutants Capturing in Wastewater[J]. ACS Ap plied Materials & Interfaces, 2013, 5(16): 8058-8066

[34] Zhang M., Wang L. W., Zeng T. Y., et al. Two pure MOF-photocatalysts with readilypreparation for the deg radation of methylene blue dye under visible light[J]. Dalton Transactions, 2018, 47(12): 4251-4258.
[35] Huitle M., Carlos A., Rodrigo M. A., et al. Single and Coupled Electrochemical Processes and Reactors for t he Abatement of Organic Water Pollutants: A Critical Review[J]. Chemical Reviews, 2015, 115(24): 13362-13407.
[36] Tompkins E. R., Mayer S. W., Ion Exchange as a Separations Method. ⅠⅠⅠ. Equilibrium Studies of the Reacti ons of Rare Earth Complexes with Synthetic Ion Exchange Resins[J]. Journal of the American Chemical Soc iety, 1947, 69(11): 2859-2865.
[37] Gao L., Li C. Y., Chan K. Y., et al. Metal-Organic Framework Threaded with Aminated Polymer Formed in Si tu for Fast and Reversible Ion Exchange[J]. Journal of the American Chemical Society, 2014, 136(20): 7209 -7212.
[38] Abherve A., Clemente-Leon M., Coronado E., et al. One-Dimensional and Two-Dimensional Anilate-Based Magnets with Inserted Spin-Crossover Complexes[J]. Inorganic Chemistry Inorg, 2014, 53 (22): 12014-120 26.
[39] Yin Z., Wan S., Yang J., et al. Recent advances in post-synthetic modification of metal-organic frameworks: New types and tandem reactions[J]. Coordination Chemistry Reviews, 2017, 378: 500-512.
[40] Zeng J. Y., Li Z., Jiang H., et al. Progress on photocatalytic semiconductor hybrids for bacterial inactivation [J]. Materials Horizons, 2021, 8(11): 2964-3008.